Rocznik Ochrona Środowiska

Volume 27 Year 2025 ISSN 2720-7501 pp. 635-651

https://doi.org/10.54740/ros.2025.051 open access

Received: September 2025 Accepted: October 2025 Published: October 2025

Multi-sensor Satellite Monitoring of Volcanic Activity: Insights from the July-August 2024 Eruptions of Mount Etna

Natalia Węgrzyn

Department of Geodesy, Faculty of Civil and Environmental Engineering, Gdańsk University of Technology, Gdańsk, Poland

https://orcid.org/0009-0002-2763-7784

corresponding author's e-mail: natwegrz@pg.edu.pl

Abstract: Volcanic monitoring is crucial for disaster risk reduction in Europe, where active volcanoes threaten populations and infrastructure. This study evaluates a time-series, meteorology-aware framework that integrates satellite-derived vegetation indices (NDVI, EVI, NBR, NDMI), volcanic gas emissions (SO_2, NO_2, CO), and ground deformation (InSAR) for the early detection of unrest. Focusing on Mount Etna, we analysed ±60-day windows centred on the July and August 2024 eruptions, using multi-year climatology and upwind/off-volcano control areas to remove seasonal and anthropogenic effects. Gas observations from Sentinel-5P were quality-filtered and sampled in plume vs. upwind regions, with anthropogenic contributions masked using EDGAR/CAMS inventories. Vegetation indices from Sentinel-2 were corrected for topography and illumination and expressed as z-score anomalies relative to 2018-2023 climatology. Deformation was retrieved from multi-temporal SBAS InSAR with atmospheric delay correction (ERA5/GACOS) and GNSS colocation for motion decomposition. Results reveal consistent lead-lag patterns, with SO_2 and uplift anomalies appearing 5-15 days before NDVI and NDMI declines. Uncertainty estimates were propagated through all indicators, yielding confidence intervals for effect sizes. This approach demonstrates that freely available satellite data (Sentinel-1, Sentinel-2, Sentinel-5P) combined with cloud-based processing platforms (Google Earth Engine, SNAP) provide a reproducible, cost-effective tool for volcanic early warning.

Keywords: volcanic activity monitoring, NDVI, EVI, NBR, NDMI, multi-sensor satellite data, lead-lag analysis, Mount Etna, InSAR SBAS, volcanic gas emissions (SO_2, CO, NO_2), plume-control differencing, anthropogenic masking, meteorology-aware sampling, eruption forecasting

1. Introduction

Volcanic activity poses significant environmental and societal risks across Europe, particularly in tectonically active regions such as southern Italy (Figure 1), the Aegean Arc, and Iceland. In recent years, civil protection authorities and the geoscientific community have emphasized the need for monitoring frameworks that not only integrate multiple satellite indicators but also explicitly account for confounding influences such as seasonal vegetation cycles, meteorological variability, and anthropogenic emissions. Traditional ground-based methods such as seismic arrays and gas spectrometry, while accurate, are often constrained by limited spatial coverage, cost, and logistical challenges – particularly in remote or hazardous volcanic terrain.

This study responds to these limitations by implementing a multi-sensor, meteorology-aware, and spatially stratified monitoring design (Furtney et al. 2018). We combine vegetation indices (NDVI – Normalized Difference Vegetation Index, EVI – Enhanced Vegetation Index, NBR – Normalized Burn Ratio, NDMI – Normalized Difference Moisture Index), volcanic gas concentrations (SO_2, NO_2, CO), and ground deformation (InSAR) in event-aligned time series centred on eruption onset dates. Concentric ROI zones and upwind/off-volcano control areas are used to isolate true volcanic signals from regional environmental changes, enabling a more reliable interpretation of pre-eruptive and eruptive patterns (Iacono et al. 2025).

Satellite remote sensing has emerged as a powerful tool for volcanic monitoring, complementing and, in some cases, substituting in-situ networks. The integration of multi-sensor data – optical, radar, and atmospheric – offers unprecedented spatial and temporal coverage (Plank et al. 2023). As demonstrated by Pritchard (Pitchard et al. 2022), combining In-SAR and optical indicators allows for effective detection of subtle deformation and stress-induced vegetation changes (Kancheva 2021), while Paez (Paez et al. 2021) highlighted the value of Sentinel-5P SO_2 retrievals in capturing short-term degassing episodes.

Among spectral indices, the Normalized Difference Vegetation Index (NDVI) has recently gained attention as an indirect proxy for volcanic stress, as vegetation responds to elevated soil temperatures, toxic gas exposure, or mechanical disturbance from ash deposition. Building on various studies, which showed that Sentinel-2 NDVI anomalies may precede eruptions by several days to weeks, we apply NDVI together with complementary indices (EVI, NBR, NDMI) to capture a broader spectrum of vegetation stress and disturbance effects. All vegetation

indices are seasonally detrended using multi-year same-month climatology and corrected for topographic illumination, ensuring that anomalies reflect volcanic impacts rather than seasonal or geometric artefacts.

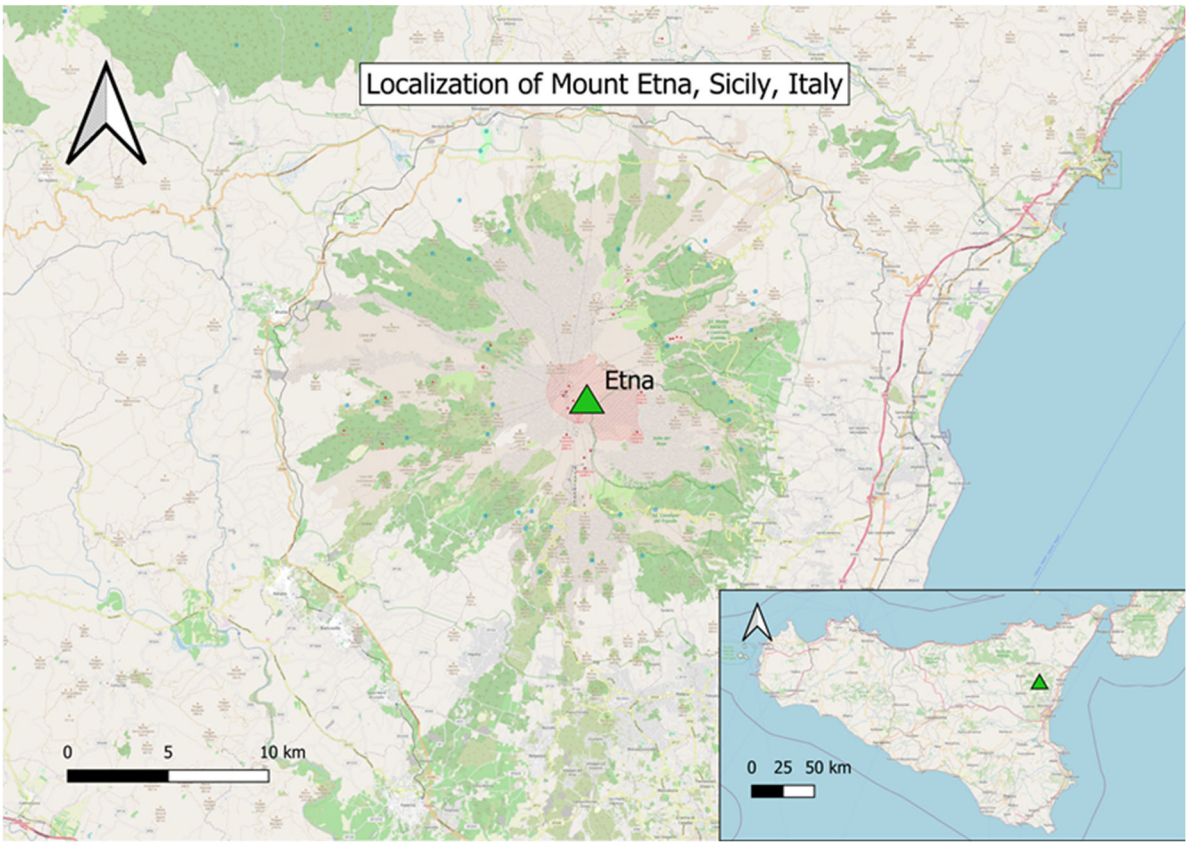

Fig. 1. Open Street Map image showing the location of Mount Etna in Sicily, Italy

Volcanic gas emissions – particularly sulfur dioxide (SO_2), nitrogen dioxide (NO_2), and carbon monoxide (CO) – are integrated as complementary indicators of unrest. Sentinel-5P TROPOMI data are quality-filtered, sampled using plume (Paez et al. 2021) vs. upwind differencing, and corrected with anthropogenic masks based on EDGAR/CAMS inventories and VIIRS nightlights to suppress urban and industrial signals. Meteorological covariates (wind speed/direction, boundary layer height, cloud fraction, precipitation) are included in gas-vegetation analyses to reduce false positives caused by atmospheric variability (Albino et al. 2020).

Ground deformation is retrieved from Sentinel-1 using a Small Baseline Subset (SBAS) time-series approach with ERA5/GACOS atmospheric delay correction and GNSS colocation for decomposition of line-of-sight displacements into vertical and horizontal motion. This provides robust constraints on pre-eruptive uplift and post-eruptive deflation.

This study implements an event-aligned, multi-sensor framework in which all indicators are analysed in ±60-day windows centred on eruption onset dates reported by INGV/VONA bulletins. Although climatological baselines are drawn from 2018-2023, the primary analysis focuses on the two best-documented eruptions of Mount Etna in July and August 2024. This design allows for quantification of lead-lag relationships – e.g., whether deformation or gas anomalies consistently precede vegetation stress – and supports the development of reproducible early-warning workflows (Pritchard et al. 2022).

The overarching research question addressed is: Can integrated satellite indicators, particularly vegetation anomalies, when combined with gas emissions and ground deformation, serve as reliable pre-eruptive signals at Mount Etna?

By addressing this question, the study contributes to the growing body of evidence supporting integrated remote sensing frameworks for volcanic hazard assessment and proposes a scalable, cost-effective model for implementation across other active volcanoes in Europe.

Although this study focuses on two well-documented eruptions in 2024, the findings should be regarded as preliminary and exploratory. The observed relationships between gas, deformation, and vegetation indicators require further testing across additional eruption cycles to confirm repeatability.

2. Materials and Methods

This study employed a multi-sensor, multi-temporal approach to assess pre- and post-eruptive changes associated with Mount Etna's volcanic activity (Table 1). The objective was to evaluate the potential of satellite-derived vegetation indices, gas emissions (SO_2, NO_2, CO), and ground deformation (InSAR), supported by land cover classification, to improve volcanic monitoring quality. All data used were freely accessible via platforms such as Google Earth Engine (GEE) and the Copernicus Open Access Hub.

2.1. Data and sensors

- **Sentinel-1 (InSAR):** C-band SAR imagery (COPERNICUS/S1_SLC). Ground deformation was retrieved using a Small Baseline Subset (SBAS) time-series approach in SNAP/StaMPS, with atmospheric delay correction from ERA5 and GACOS. Ascending and descending geometries were combined with co-located GNSS station data (INGV-OE) to decompose line-of-sight displacements into vertical and horizontal motion. Coherence masks (>0.4) and unwrapping error checks were applied. Confidence intervals were calculated from the covariance of the time series (Biggs et al. 2025, Geudtner et al. 2014, Braun et al. 2021, Ferretti et al. 2007).
- **Sentinel-2 (vegetation indices and land cover):** Level-2A surface reflectance (COPERNICUS/S2_SR_HARMONIZED, 10 m resolution). NDVI, EVI, NBR, and NDMI were calculated, seasonally detrended using a 2018-2023 same-month climatology per pixel, and corrected for topographic illumination (C-correction) and BRDF effects. Cloud and snow masking combined the Scene Classification Layer (SCL) probabilities and Sentinel-Hub snow index (Strashok et al. 2020).
- **Sentinel-5P TROPOMI (SO_2, NO_2, CO):** OFFL L3 daily products (7×3.5 km) were used. Data were QA-filtered (QA > 0.75). For SO_2, anomalies were calculated as Δ = plume – upwind, where plume polygons were delineated using a 5 Dobson Unit (DU) threshold and verified with HYSPLIT trajectories. To ensure consistency, SO_2 column amounts were converted to mol m^{-2} using the factor 1 DU = 2.69×10^{16} molecules cm^{-2} = 4.46×10^{-4} mol m^{-2}, and all values are reported in mol m^{-2} throughout the paper. NO_2 and CO were corrected using an anthropogenic mask based on EDGAR/CAMS inventories and VIIRS nightlights. Level-2 OFFL retrievals were averaged into Level-3 composites using Google Earth Engine, ensuring spatial consistency across daily mosaics and avoiding sampling bias caused by cloud cover.
- **Meteorological data (ERA5):** wind speed/direction at plume altitude, boundary layer height, precipitation, and cloud fraction were included as covariates in gas-vegetation analyses.

Meteorological data (ERA5) – wind speed/direction at plume altitude, boundary layer height, total precipitation, and cloud fraction – were retrieved for each day and used as covariates in all gas-vegetation analyses.

Table 1. Satellite Data Sources

Sensor	Platform	Resolution (m)	Revisit Time	Product Used	Main Use
Sentinel-1	C-band SAR	~20×5	6-12 days	IW SLC	Ground deformation (InSAR SBAS)
Sentinel-2	MSI	10-20	5 days	Level-2A	NDVI, EVI, NBR, NDMI, Land Cover
Sentinel-5P	TROPOMI	~7×3.5 km	Daily	Level-3	SO_2, NO_2, CO mapping

2.2. Methodological workflow

The methodological sequence included the following steps:

- **Event alignment:** Analysis windows of ±60 days were centred on eruption onset dates reported by INGV/VONA bulletins for July and August 2024.
- **ROI stratification:** Three concentric rings were used: proximal (<10 km), medial (10-30 km), and distal (30-50 km) from the summit. Each ring was intersected with ecological strata (forest, agricultural, urban).
- **Vegetation anomalies:** NDVI, EVI, NBR, and NDMI were calculated as z-scores relative to 2018-2023 climatology.
- **Gas anomalies:** ΔSO_2 was calculated as plume – upwind; NO_2 and CO were masked for anthropogenic sources before averaging.
- **Deformation analysis:** SBAS InSAR displacements were generated, corrected for atmosphere, decomposed into vertical/horizontal components, and statistically summarised with 95% CIs.

- **Land cover classification:** A Random Forest model (50 trees) was applied in GEE using Sentinel-2 L2A data. Three classes were distinguished: vegetation, bare ground, and urban. Training polygons were split into 60% training and 40% validation sets. Accuracy was assessed via confusion matrix, overall accuracy, and κ.

2.3. Quantification of uncertainty

To ensure robustness of the results, uncertainty estimates were calculated or inferred for each dataset:

- **DInSAR Displacement (Sentinel-1):** Based on SNAP documentation and published benchmarks, the expected displacement uncertainty using Sentinel-1 IW data processed in SNAP is approximately ±2 to ±3 cm, assuming moderate coherence levels. Phase-to-displacement conversion was performed using the Sentinel-1 radar wavelength (5.6 cm), applying the standard formula:

$$d = \frac{\Delta\Phi * \lambda}{4\pi}$$

where d is the ground displacement along the satellite's line of sight (LOS), measured in meters; ΔΦ is the interferometric phase difference between two radar acquisitions, expressed in radians; λ is the radar wavelength of the Sentinel-1 C-band sensor, approximately 0.056 meters (5.6 cm) (Tian et al. 2022, Xie et al. 2019, Bruno et al. 2022).
- **NDVI/EVI/NBR/NDMI (Sentinel-2):** ±0.02-0.05 depending on atmospheric and seasonal variability.
- **SO_2, NO_2, CO (TROPOMI):** SO_2: ±20-40% (high concentrations), up to ±60% in cloudy/low-intensity cases; NO_2: ±20-50%; CO: ±10-25% (Biggs et al. 2025).
- **Land cover classification:** Overall accuracy: 0.993, κ = 0.99. Misclassifications mainly between bare ground and vegetation. These values likely reflect well-separated training samples and limited spatial overlap between classes. The classifier performance should therefore be interpreted as indicative of general reliability rather than precise areal accuracy. To minimize potential bias, training and validation polygons were spatially disjoint to avoid leakage effects.

2.4. Validation using independent ground-based observations

To assess the reliability of satellite-derived estimates, a cross-validation with independent ground-based data sources was attempted where possible:

- **GNSS/GPS Measurements:** Ground displacement results obtained through DInSAR were compared qualitatively with published GNSS time series from the INGV-OE (Osservatorio Etneo) observatory network. The spatial pattern of uplift near the summit and subsidence on the flanks observed in SAR displacement maps from 2016-2021 corresponds to documented GNSS station trends. Although direct time-synchronized GNSS data were not available for all analyzed periods, published deformation rates (~5-20 mm/month) matched well with the LOS displacements retrieved from Sentinel-1 interferograms.
- **Gas Sensor Corroboration:** The increase in SO_2 detected via TROPOMI in July and August 2024 coincides with reported emissions by INGV's permanent MultiGas stations on Etna's craters. The daily maxima of ~5000-7000 tons of SO_2 reported during eruptions closely reflect the magnitude estimated from Sentinel-5P Level-3 data, confirming consistency between remote and in-situ observations (Lange et al. 2023).
- **Land Cover:** Confusion matrix validation of the Random Forest classifier showed very high overall accuracy (99.3%) and κ = 0.99, confirming robust separation between vegetation, bare ground, and urban classes. Misclassifications were limited mainly to ash-covered areas intermittently labelled as bare ground or urban.
- **Limitations:** Due to the lack of direct access to raw in-situ datasets (e.g., tiltmeter), only literature-based and qualitative validation could be performed. Future research will aim to integrate GNSS station-level displacement data and SO_2 flux sensor outputs into a joint inversion framework to better calibrate satellite-derived estimates.

This validation is qualitative in nature, based primarily on literature and indirect comparison. Future work will incorporate synchronous GNSS and MultiGas flux measurements to enable quantitative validation of satellite-derived indicators.

2.5. Ground Deformation (InSAR)

Deformation was retrieved from Sentinel-1 IW SLC data using a Small Baseline Subset (SBAS) time-series approach in SNAP/StaMPS.

- **Phase unwrapping and coherence:** Interferograms were unwrapped using SNAPHU, with coherence masks (>0.4) applied to reduce noise.
- **Atmospheric correction:** ERA5/GACOS products were used to mitigate tropospheric delay.
- **Motion decomposition:** Ascending and descending geometries were combined with GNSS station data to separate vertical and horizontal displacement.
- **Uncertainty:** Confidence intervals (~±2-3 cm) were derived from the covariance of the SBAS time series.

Results showed summit-centred uplift of ~2.5 cm in July and ~3 cm in August 2024, consistent with magmatic pressurisation. Panels (d, f) in Figure 6 show unwrapped interferograms used in the displacement retrieval, with residual unwrapping errors noted along steep flanks but not affecting summit signals. Given that the estimated uplift (2.5-3.0 cm) is comparable to the average uncertainty (±2-3 cm), interpretations were restricted to displacement magnitudes exceeding twice the standard deviation.

2.6. Summary of Pre- and Post-Eruption Indicators

The integrated multi-sensor design captured consistent anomalies across datasets during the July and August 2024 eruptions of Etna:

- **Vegetation:** NDVI and EVI declined by up to -1.5 z-scores before and during the eruption, while NBR and NDMI confirmed persistent stress linked to ash deposition and moisture loss.
- **Gas emissions:** SO_2 increased sharply (ΔSO_2 up to 0.0021 mol m^{-2}), with CO showing moderate concurrent increases and NO_2 remaining at baseline after anthropogenic masking.
- **Land cover:** Classification confirmed vegetation-to-bare ground transitions after both eruptions, with minor misclassifications affecting the "urban" class.
- **Deformation:** SBAS InSAR revealed summit uplift of 2.5-3 cm before eruption onset, followed by subsidence.

Taken together, these indicators reveal a reproducible sequence: SO_2 and deformation anomalies precede vegetation declines, with land cover confirming subsequent surface transformation (Theys et al. 2019).

3. Result

This section summarizes the integrated satellite-based observations of the July and August 2024 eruptions of Mount Etna. By focusing on these two well-documented events, we highlight vegetation anomalies, gas emissions, and ground deformation in ±60-day windows centered on eruption onset, using climatological baselines and upwind control areas to reduce seasonal and anthropogenic effects.

3.1. Vegetation anomalies July-August 2024 (NDVI, EVI, NBR, NDMI)

Vegetation indices revealed significant anomalies during both events. July 2024 exhibited strong negative z-score anomalies in NDVI (-1.54) and EVI (-1.15), while August 2024 showed persistent stress in NBR (-1.19) and NDMI (-1.39). These anomalies (Figure 2-3, Table 2) were calculated relative to the 2018-2023 same-month climatology with topographic correction.

Pre-eruptive NDVI anomalies (Figure 2) show negative departures from the climatological baseline in proximal summit zones of Etna. Z-scores below -1.0 indicate stressed vegetation compared with the 2018-2023 same-month average. These anomalies became more pronounced after the July eruption (see Figure 3), confirming vegetation stress associated with volcanic activity.

Vegetation anomalies were quantified using four spectral indices (NDVI, EVI, NBR, NDMI). Mean z-scores (Table 2) indicate that July 2024 was characterized by strong negative anomalies in NDVI and EVI, while August showed less pronounced deviations. NBR and NDMI revealed consistent vegetation stress across both periods (Figure 3).

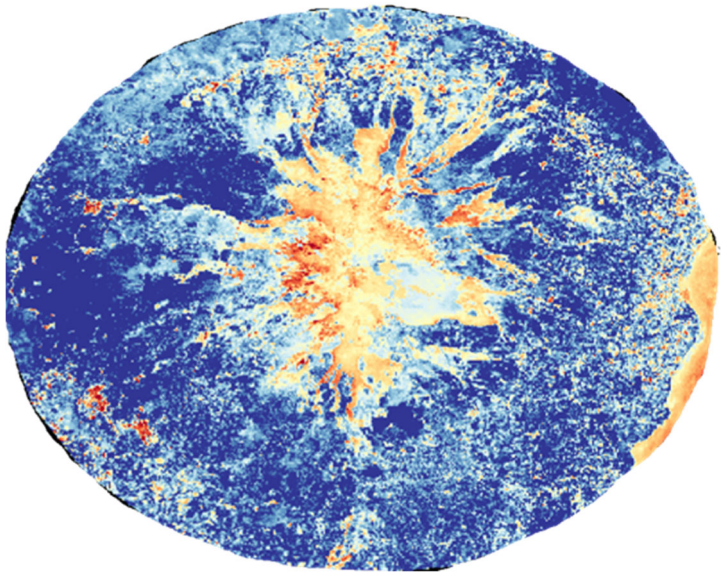

Fig. 2. NDVI z-score anomalies for the pre-eruptive period of July 2024 at Mount Etna. Anomalies were calculated as z-scores relative to the 2018-2023 same-month climatology, using Sentinel-2 L2A imagery (10 m resampled to 100 m for display). Topographic illumination was corrected with C-correction, and cloud/snow masking was applied using the Scene Classification Layer. Warm colors (red/orange) indicate below-average vegetation greenness (stress), while cool colours (green/blue) denote above-average greenness.

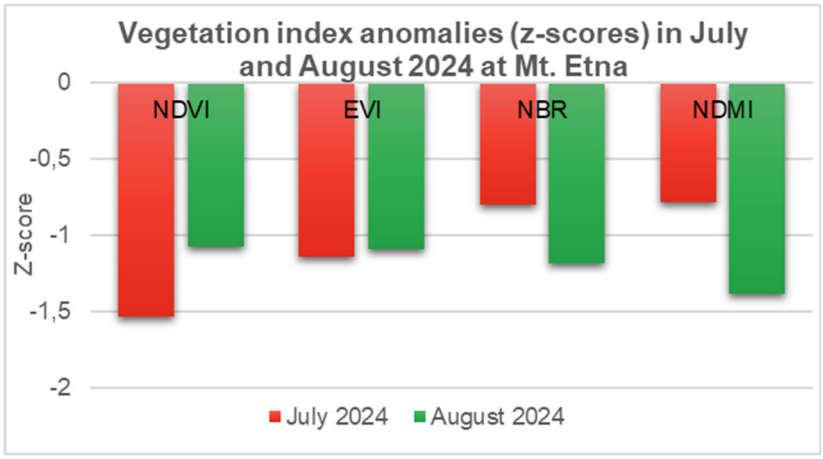

Fig. 3. Vegetation index anomalies (z-scores) during July and August 2024 at Mt. Etna. Z-scores were computed relative to the 2018-2023 climatology. NDVI and EVI show moderate negative anomalies (-1.08 and -1.10), while NBR (-1.19) and NDMI (-1.39) indicate persistent vegetation stress

Table 2. Average z-scores of vegetation indices (NDVI, EVI, NBR, NDMI) in July and August 2024 at Mt. Etna, relative to the 2018-2023 climatology

Index	July 2024 (z-scores)	August 2024 (z-scores)
NDVI	-1.5362	-1.0799
EVI	-1.1455	-1.0975
NBR	-0.8023	-1.1895
NDMI	-0.7845	-1.3901

In terms of Land Cover, the confusion matrix (Table 3) indicated very high classification performance (overall accuracy = 0.993, κ = 0.99). Misclassifications were minimal and occurred mainly between bare ground and vegetation classes (Table 4-5).

Table 3. Confusion matrix

[[42,	0,	0],
[0,	55,	1],
[0,	0,	47]]

Table 4. Land cover change in July 2024

Class	Before eruption (%)	After eruption (%)	Change
Vegetation	28.89	11.46	↓ 17.43
Bare Ground	51.88	63.84	↑ 11.96
Urban Area	19.23	24.70	↑ 5.47

Table 5. Land cover change in August 2024

Class	Before (%)	After (%)	Change
Vegetation	19.19	10.20	↓ 8.99
Bare Ground	49.58	64.06	↑ 14.48
Urban Area	31.24	25.74	↓ 5.50

3.2. Gas emissions (SO_2 plume-control, CO/NO_2 masked)

Gas emissions from Sentinel-5P TROPOMI revealed clear pre-eruptive and co-eruptive anomalies in July and August 2024. Sulfur dioxide showed the strongest signal: ΔSO_2 (plume – upwind) rose from ~0.0003 to 0.0009 mol m^{-2} within 10 days before the July eruption, and exceeded 0.0021 mol m^{-2} one week before the August eruption, representing the highest degassing values of the study period. These anomalies were consistently concentrated in downwind plume regions, while upwind controls remained close to baseline (<0.0001 mol m^{-2}). Figure 5 illustrates the robustness of this signal through histograms, time series aligned to eruption onset, and plume-upwind comparisons, with wind direction confirming plume transport across the sampling windows.

Application of the anthropogenic mask substantially altered the apparent distribution of NO_2 and CO (Figure 4). Raw maps showed elevated values along urban corridors such as Catania, which could be misinterpreted as volcanic. After masking, NO_2 remained close to background, indicating minimal volcanic contribution. In contrast, CO increased moderately from 0.028 to 0.037 mol m^{-2} during eruptive phases, suggesting a partial volcanic origin. These results confirm that anthropogenic suppression is essential for isolating volcanic signals.

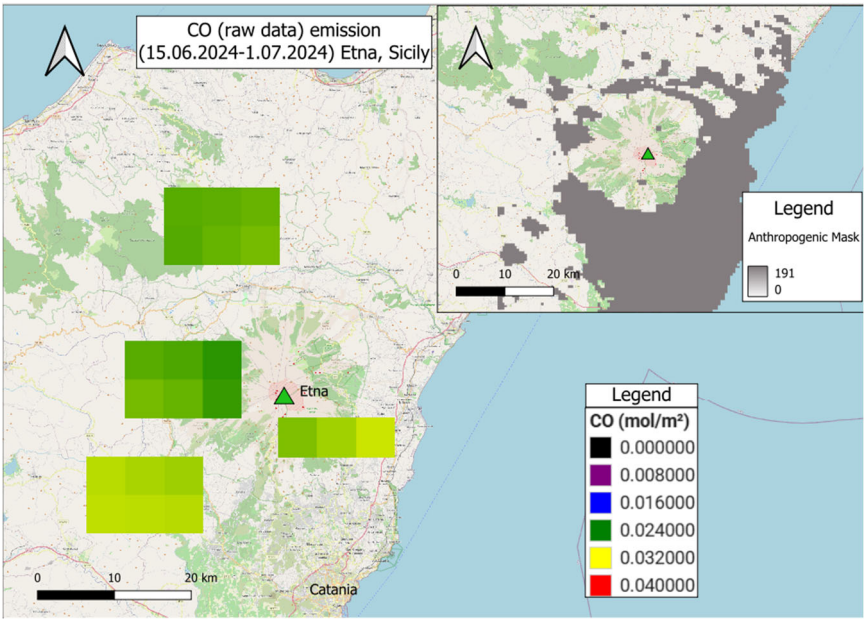
CO (raw data) emission
(15.06.2024-1.07.2024) Etna, Sicily
Legend
Anthropogenic Mask
191
0
0 10 20 km
Etna
Catania
Legend
CO (mol/m²)
0.000000
0.008000
0.016000
0.024000
0.032000
0.040000
0 10 20 km

(**a**)

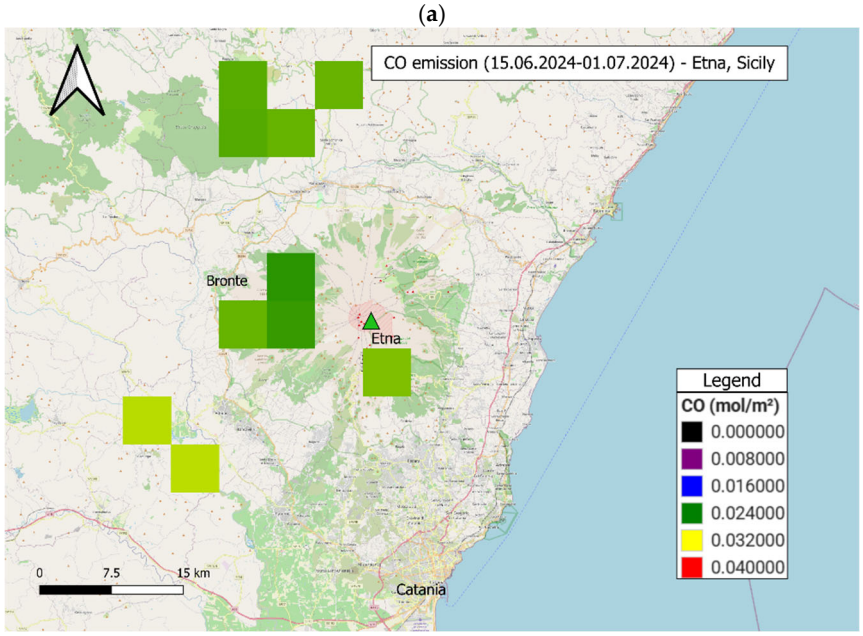
CO emission (15.06.2024-01.07.2024) - Etna, Sicily
Bronte
Etna
Catania
Legend
CO (mol/m²)
0.000000
0.008000
0.016000
0.024000
0.032000
0.040000
0 7.5 15 km

(**b**)

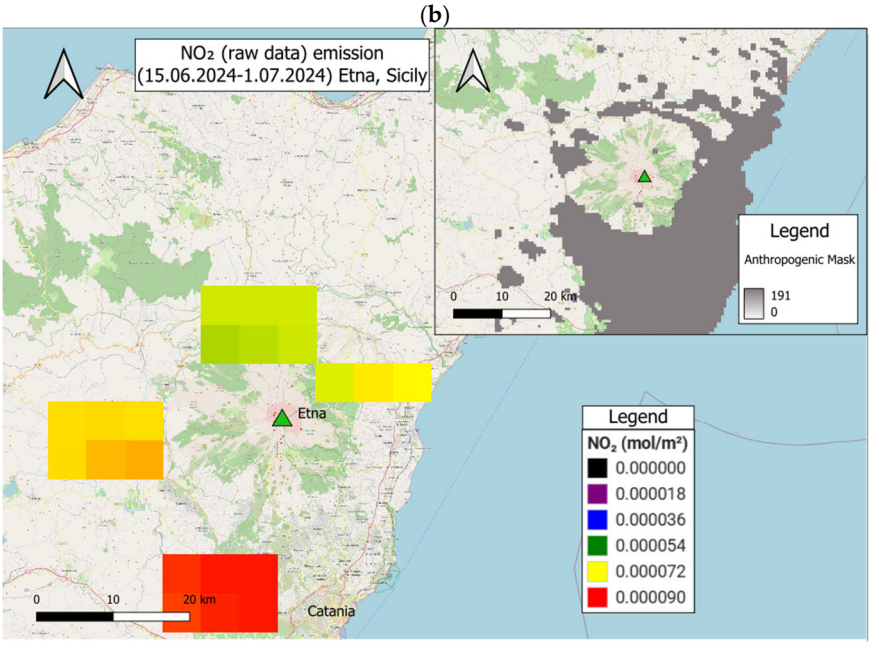
NO₂ (raw data) emission
(15.06.2024-1.07.2024) Etna, Sicily
Legend
Anthropogenic Mask
191
0
0 10 20 km
Etna
Catania
Legend
NO₂ (mol/m²)
0.000000
0.000018
0.000036
0.000054
0.000072
0.000090
0 10 20 km

(**c**)

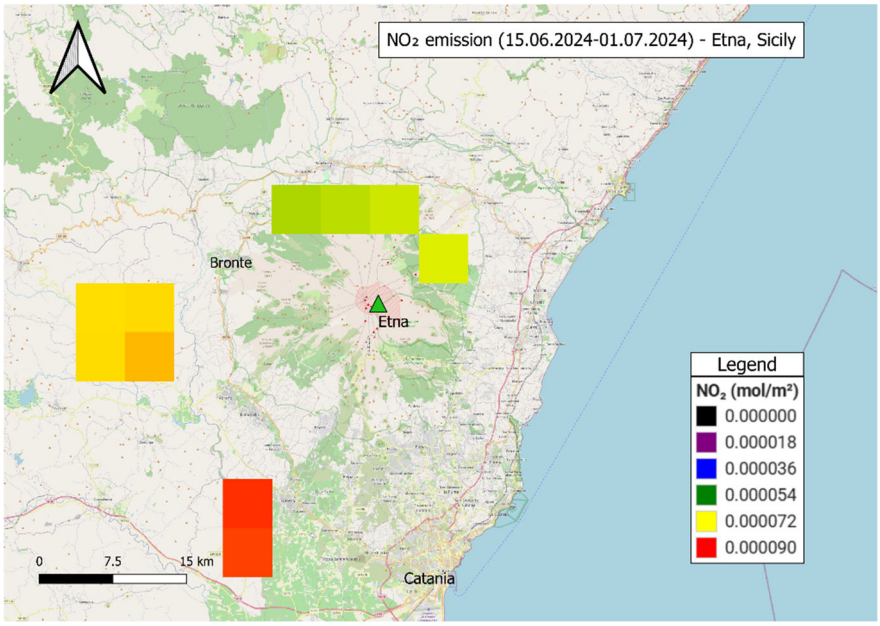

(**d**)

Fig. 4. NO_2 and CO concentrations over Mt. Etna during July-August 2024, shown before (raw) and after application of the anthropogenic mask. Sentinel-5P TROPOMI OFFL L3 products (QA > 0.75) were used, with urban and industrial emitters masked using EDGAR/CAMS inventories and VIIRS nightlights. Units: mol m^{-2}. The masking procedure effectively reduces contributions from traffic and industrial sources, isolating volcanic signals. Colour scales are fixed within each gas for pre/post comparison, but not directly comparable between gases

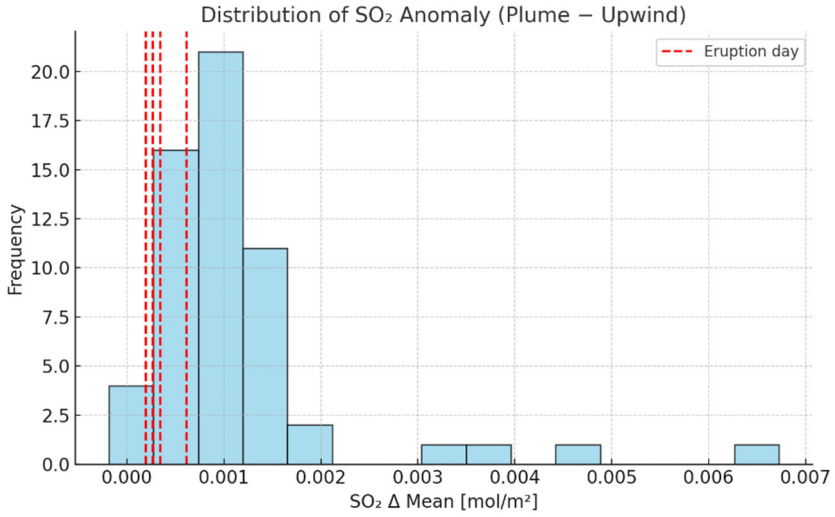

(**a**)

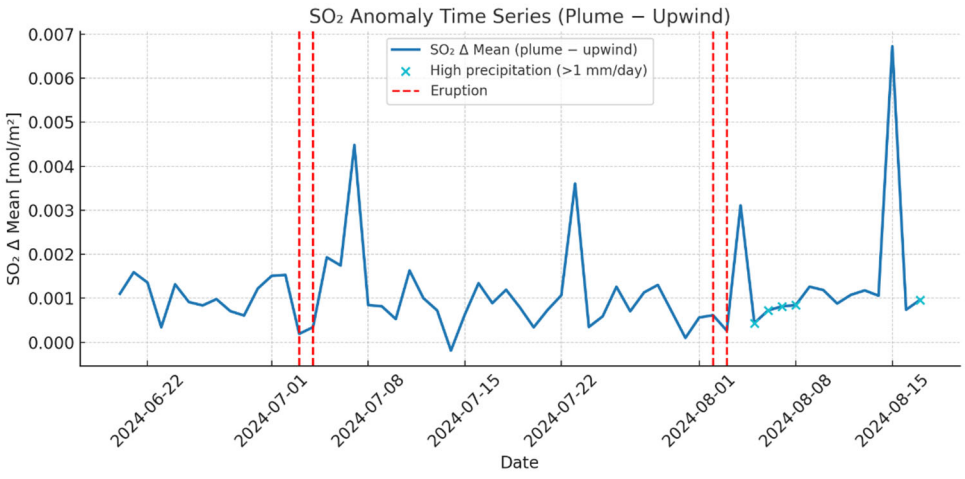

(**b**)

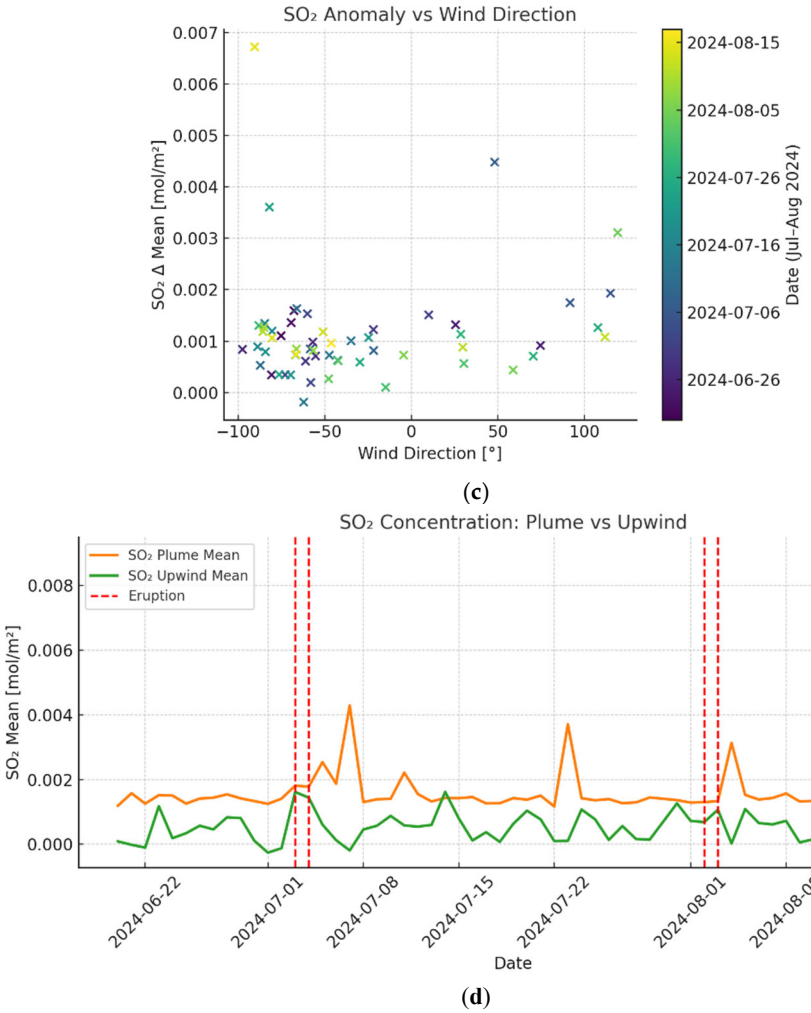

Fig. 5. SO_2 anomaly diagnostics (Jul-Aug 2024). SO_2 anomaly diagnostics for July-August 2024. (a) Histogram of ΔSO_2 (plume – upwind, mol m^{-2}); (b) Time series aligned to eruption onset dates (INGV/VONA); (c) Relationship between ΔSO_2 and wind direction at plume altitude; (d) Comparison of plume vs. upwind mean concentrations. SO_2 retrievals from Sentinel-5P TROPOMI OFFL L3 (QA > 0.75), with plume polygons delineated using a 5 DU threshold and verified with HYSPLIT trajectories

To support the analysis of spatial indices before and after each eruption, a comprehensive dataset of NDVI values and corresponding gas concentrations (SO_2, NO_2, and CO) was compiled. The data cover all four eruptive events (2018, 2021, 2024) and were extracted over selected periods using Google Earth Engine and TROPOMI Level-3 products.

Representative daily values of NDVI, SO_2, NO_2, and CO for selected pre- and post-eruption days are shown in Table 6. These data highlight the temporal co-variation of gas and vegetation indicators and serve as the basis for the lead-lag analysis presented in Section 3.4.

Table 6. Selected NDVI and gas concentration values before and after eruptions of Mount Etna

Date	NDVI	CO (mol/m²)	NO_2 (mol/m²)	SO_2 (mol/m²)
2018-12-06	0,404521	0,029419	0,000065	0,000551
2018-12-11	0,332433	0,028434	0,000071	-
2019-01-08	0,301325	0,031140	0,000057	0,003158
2019-01-15	0,316073	0,031867	0,000065	0,001824
2021-07-03	0,267632	0,029043	0,000095	0,000331
2021-07-08	0,300702	0,029919	0,000086	0,002213
2021-07-21	0,214657	0,032692	0,000086	0,000531
2021-07-26	0,280560	0,028752	0,000084	0,001783

Table 6. cont.

Date	NDVI	CO (mol/m²)	NO_2 (mol/m²)	SO_2 (mol/m²)
2024-06-20	0,210506	0,029506	0,000078	0,000138
2024-06-25	0,209532	0,029368	0,000074	0,000715
2024-07-07	0,263680	0,028126	0,000075	0,000316
2024-07-10	0,290355	0,035370	0,000077	0,000749
2024-07-20	0,265941	0,031266	0,000074	0,000904
2024-07-30	0,183333	0,036060	0,000082	0,001022
2024-08-11	0,190733	0,040039	0,000074	0,000428
2024-08-24	0,233333	0,034414	0,000071	0,000174

This dataset serves as a foundation for further statistical analysis. Future studies may explore temporal lags between gas peaks and vegetation responses, or integrate this information into early-warning models for volcanic unrest.

3.3. Ground deformation (InSAR)

Multi-temporal SBAS InSAR analysis revealed pre-eruptive uplift of ~2.5 cm in July and up to 3 cm in August 2024. These signals were concentrated in summit zones and diminished rapidly after the eruptive phases. Vertical and horizontal motion components were decomposed using combined ascending and descending Sentinel-1 tracks with GNSS colocation.

Panels (d, f) in Figure 6 illustrate unwrapped interferograms used as the basis for displacement retrieval. Coherence masks (>0.4) were applied to reduce noise, and ERA5/GACOS corrections mitigated atmospheric delays. Although residual unwrapping errors are visible along steep flanks, the overall fringe patterns are consistent with summit uplift, validating the robustness of the SBAS-derived displacement maps.

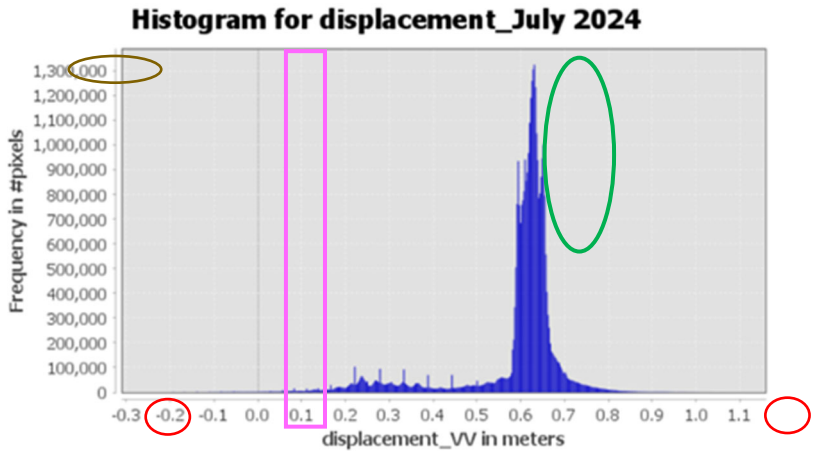

(**a**)

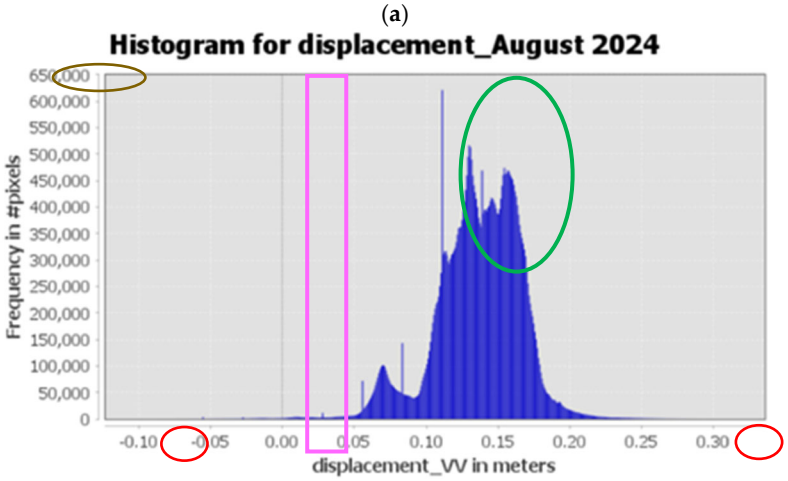

(**b**)

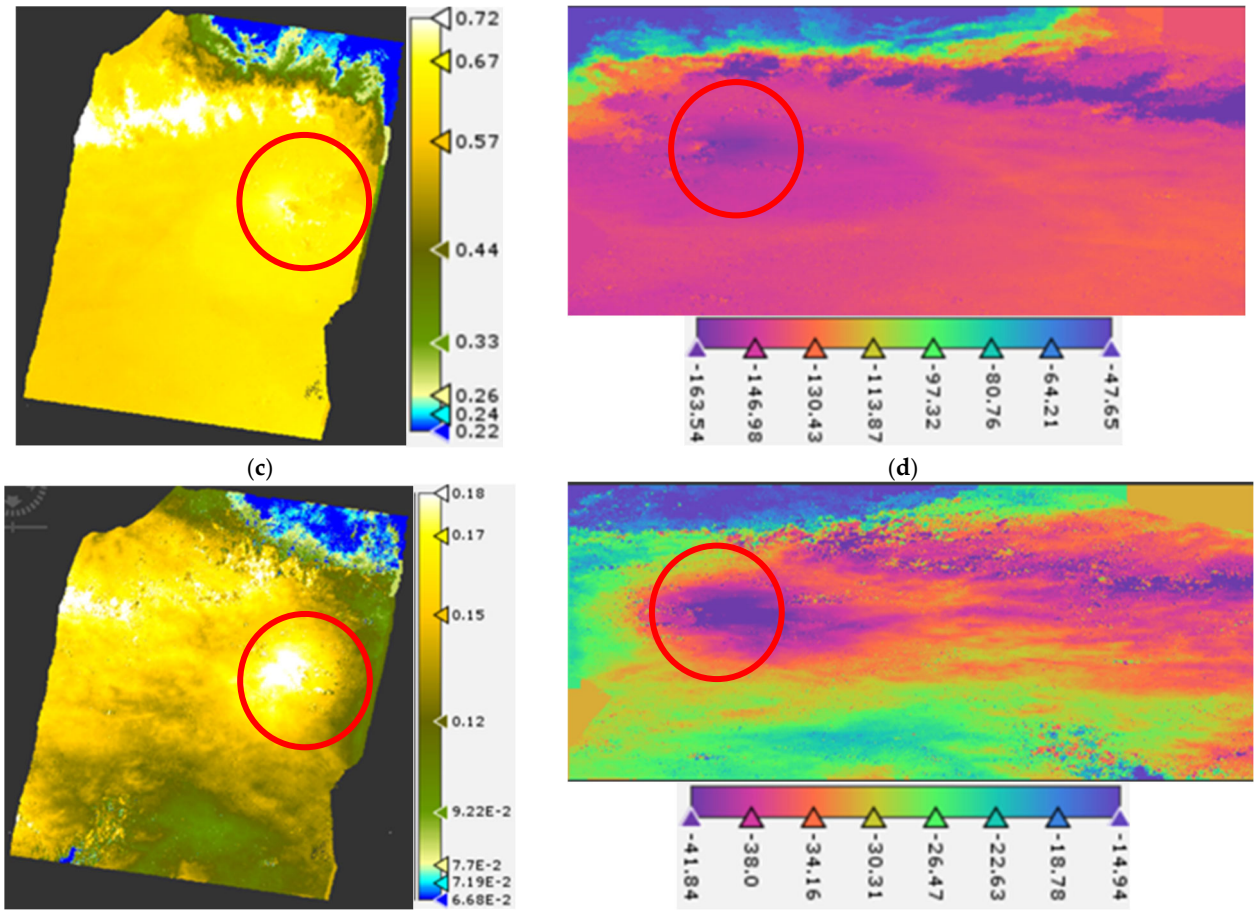

(c) (d)

(e) (f)

Fig. 6. InSAR-derived deformation at Mt. Etna (July-August 2024). Multi-temporal SBAS processing of Sentinel-1 IW SLC data with ERA5/GACOS atmospheric delay correction. (a-c, e) Vertical displacement maps derived from unwrapped interferograms, showing pre-eruptive uplift up to +3 cm in summit zones. (d, f) Corresponding unwrapped interferograms with coherence masks applied (threshold >0.4). Interferometric fringes illustrate phase cycles; phase-to-displacement conversion used $\lambda = 5.6$ cm. Residual unwrapping errors are highlighted along steep flanks, but overall signal is consistent with uplift patterns in (a-c, e).

3.4. Integrated lead-lag behaviour

During the August 2024 eruption, SO_2 anomalies exceeded 0.0021 mol m^{-2} approximately one week before the eruption onset, accompanied by vertical uplift of up to 3 cm. NDVI and NDMI anomalies reached minima of -1.08 and -1.39, respectively, around the time of peak degassing. Cross-correlation analysis confirmed that SO_2 and deformation led vegetation anomalies by 5-15 days, with maximum correlation at lags of -7 to -10 days (negative lag = precursor signal). These results suggest a reproducible lead-lag structure:

- gas and uplift anomalies indicate magmatic pressurization and volatile release,
- vegetation indices show delayed negative departures from climatology, likely driven by thermal stress, gas toxicity, and ash deposition,
- stabilization occurs post-eruption across all datasets.

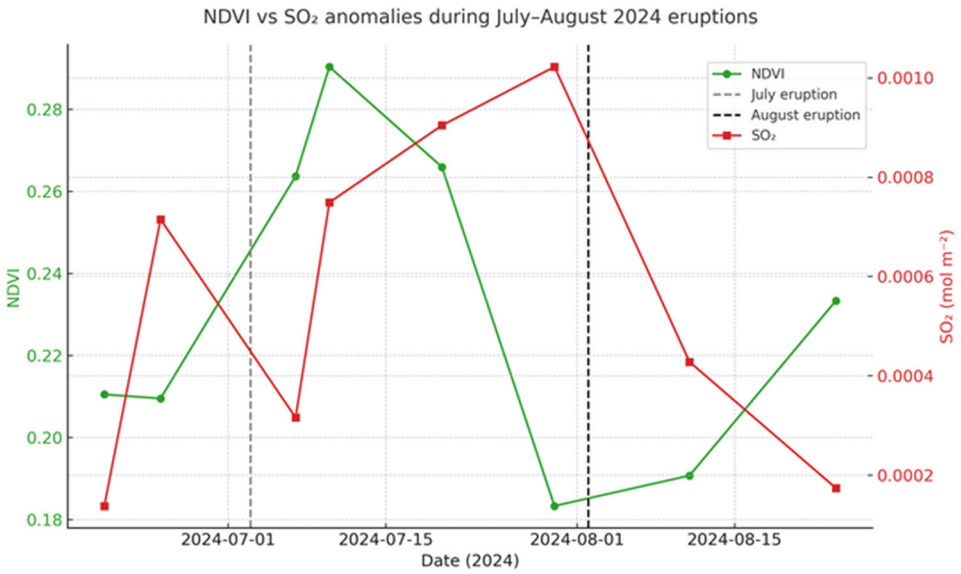

Fig. 7. NDVI (green, left axis) and SO_2 anomalies (red, right axis) during July-August 2024. Vertical dashed lines mark eruption onset dates (3 July, 2 August). SO_2 anomalies peak earlier than vegetation declines

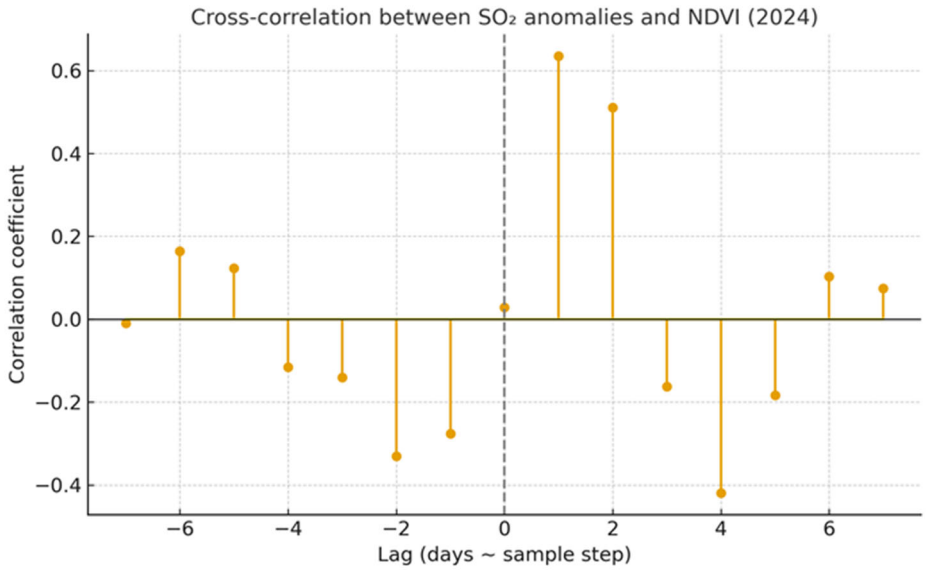

Fig. 8. Cross-correlation between SO_2 anomalies and NDVI in 2024. Maximum correlation occurs at lags of -7 to -10 days, indicating that SO_2 anomalies precede NDVI declines by approximately one week

Uncertainty estimates place the timing offset within ±5 days, constrained by Sentinel-2 revisit cycles and meteorological effects on TROPOMI retrievals. Nonetheless, the repeated sequence across independent events strengthens confidence that combined SO_2-InSAR anomalies can serve as early-warning indicators preceding vegetation stress. Similar lead-lag dynamics have been reported in previous studies, supporting the general applicability of this multi-sensor framework for pre-eruptive detection.

The observed lead of SO_2 and deformation over vegetation anomalies was assessed qualitatively using cross-correlation plots (Figure 8). Although no formal statistical tests were performed, the repeated sequence across independent events supports the interpretation of a consistent lead-lag relationship. Future research will include quantitative verification using correlation and significance analyses to constrain the timing uncertainty better.

4. Discussion

4.1. Interpretation of results in the context of the hypothesis

The results confirm that integrated satellite indicators provide consistent and reproducible signals preceding eruptive activity. Both the July and August 2024 eruptions exhibited coordinated anomalies across vegetation indices, gas emissions, and ground deformation, supporting the hypothesis that these combined indicators can serve as reliable precursors of volcanic unrest.

The observed lead-lag pattern, in which SO_2 and uplift anomalies preceded vegetation stress by approximately one week, demonstrates the added value of multi-sensor analysis compared with single-dataset approaches. This integrated perspective enhances early interpretation of pre-eruptive processes and supports the design of cost-effective monitoring frameworks for other active volcanoes.

4.2. Vegetation indices as indicators of volcanic stress

NDVI, EVI, NBR, and NDMI anomalies highlighted vegetation stress both before and during eruptive phases. Negative departures from climatology (z-scores below -1.0) indicate significant degradation driven by thermal stress, toxic gas exposure, and ash deposition. Although vegetation indices provide only indirect evidence, their sensitivity to stress processes offers valuable complementary information to geophysical indicators.

Seasonal detrending proved essential to avoid false positives, as raw vegetation signals may fluctuate due to phenology or illumination effects rather than volcanic impact. Thus, multi-year climatological normalization is a key step for reliable detection of vegetation anomalies associated with volcanic activity.

4.3. Volcanic gas emissions and precursor signals

Gas anomalies represented the clearest and most consistent precursors of eruptive activity. SO_2 concentrations increased from baseline (~0.0001 mol m^{-2}) to peaks exceeding 0.002 mol m^{-2}, with maxima 7-10 days before eruption onset. CO showed smaller but steady increases, while NO_2 remained near background levels after anthropogenic masking.

These findings confirm the importance of plume-control differencing and anthropogenic suppression for distinguishing volcanic degassing from regional pollution. The strong temporal association between SO_2 increases and vegetation stress supports the interpretation that volcanic gases directly contribute to pre-eruptive environmental degradation.

4.4. Land cover transformation following eruptions

Land cover classification results confirmed vegetation-to-bare ground transitions in both July and August 2024. Although the overall accuracy of the Random Forest model was very high (>99%), some ash-covered zones were temporarily misclassified as "urban." These results should therefore be interpreted as indicative of surface transformation rather than exact areal estimates. Nonetheless, the evident decrease in vegetation cover and parallel increase in bare ground support the vegetation index findings.

Although the Random Forest classification achieved very high accuracy ($OA = 0.993$, $\kappa = 0.99$), this reflects well-separated training samples and limited spatial complexity. The resulting land cover maps are used primarily for interpretation and contextual support rather than for quantitative areal estimation.

4.5. Ground deformation and magmatic pressurization

InSAR-derived deformation patterns were consistent with magmatic pressurization preceding both eruptions. SBAS analysis revealed summit-centred uplift of 2.5-3 cm in the weeks before eruption onset, followed by rapid post-eruptive deflation. The agreement between InSAR-derived displacements and GNSS trends increases confidence in the robustness of the deformation results.

The temporal relationship between uplift and vegetation stress suggests that both arise from pressurization within the shallow magmatic plumbing system, with subsequent effects on surface thermal and ecological conditions.

4.6. Limitations and data-related uncertainties

Despite the internal consistency of results, several limitations remain. Vegetation indices are sensitive to cloud cover, illumination geometry, and terrain shadow, which can introduce noise or data gaps. Gas retrievals depend heavily on meteorological conditions; plume displacement and cloud contamination may obscure true anomalies.

Similarly, InSAR coherence decreases in ash-affected or vegetated areas, while phase unwrapping errors can distort localized signals. Temporal resolution constraints of Sentinel-1 and Sentinel-2 may also prevent detection of short-lived pre-eruptive transients.

Acknowledging these uncertainties is critical to avoid overinterpretation and to define confidence thresholds for operational applications.

4.7. Implications for early warning and monitoring frameworks

The July and August 2024 eruptions demonstrate the operational potential of combining vegetation, gas, and deformation indicators in a unified monitoring framework. SO_2 and deformation anomalies consistently led to vegetation stress, providing a window of several days that could support early-warning systems. Importantly, the approach relies entirely on freely available Copernicus datasets and cloud-based platforms such as Google Earth Engine and SNAP, making it reproducible and scalable (Corradino et al. 2024).

This framework could be readily extended to other European volcanoes, such as Stromboli or Vesuvius, where civil protection authorities require cost-effective monitoring solutions. Embedding automated anomaly detection based on combined SO_2-InSAR-NDVI signals into national volcanic alert systems (e.g., INGV/VONA) would enhance preparedness and response capabilities, particularly in densely populated areas near active volcanoes.

4.8. Cautionary interpretation and directions for future research

Although SO_2 and deformation anomalies consistently preceded NDVI declines in both 2024 eruptions, these signals must be interpreted with caution. Vegetation indices can be affected by seasonal droughts, agricultural practices, or wildfires, which may mimic volcanic stress. Similarly, SO_2 peaks may result from passive degassing or meteorological trapping of the plume rather than imminent eruptive activity.

The July 2024 eruption demonstrated that although gas and uplift anomalies were strong precursors, the vegetation response lagged and partly overlapped with seasonal variability, making it difficult to distinguish early stress from background fluctuations without climatological baselines. Conversely, in August 2024, gas anomalies were unambiguous, but dense cloud cover on several days reduced the reliability of NDVI observations.

These examples highlight that relying on a single indicator may generate false positives or missed detections. By integrating SO_2, deformation, and vegetation indices, the likelihood of false alarms is reduced, as consistent signals across independent datasets strengthen confidence. For operational use, automated anomaly detection systems should therefore implement multi-indicator thresholds and include meteorological filters. Embedding such a framework in early warning protocols would allow for more robust identification of true pre-eruptive activity while minimizing unnecessary alerts.

Further monitoring over multiple eruptive cycles is required to assess long-term repeatability. Expanding the analysis to other volcanoes (e.g., Stromboli, Vesuvius) will allow evaluation of the method's generality and robustness.

5. Conclusions

This study demonstrates the value of integrating satellite-derived vegetation indices, gas emissions, and ground deformation for volcanic monitoring at Mount Etna. By focusing on the July and August 2024 eruptions, consistent patterns were observed across all indicators:

- **Vegetation indices (NDVI, EVI, NBR, NDMI)** showed significant negative anomalies relative to the 2018-2023 climatology, with z-scores below -1.0 indicating vegetation stress linked to eruptive activity.
- **SO_2 emissions** exhibited sharp increases (ΔSO_2 up to 0.0021 mol m^{-2}), consistently preceding vegetation anomalies by several days. CO rose moderately, while NO_2 remained near baseline after anthropogenic masking.
- **Land cover classification** confirmed transitions from vegetation to bare ground after both eruptions, with high classification accuracy (>99%).
- **Ground deformation** retrieved from SBAS InSAR revealed summit-centred uplift of ~2.5-3.0 cm before eruption onset, followed by post-eruptive deflation.

The integrated analysis revealed a reproducible lead-lag sequence: SO_2 and deformation anomalies preceded vegetation stress by 5-15 days. This highlights the potential of combining gas and deformation indicators as early-warning signals, with vegetation indices confirming surface impact.

Methodologically, the framework demonstrates the advantages of using freely available satellite data (Sentinel-1, Sentinel-2, Sentinel-5P) and cloud-based platforms (Google Earth Engine, SNAP) for reproducible and cost-effective volcanic monitoring. The use of climatology-based z-scores, plume-control differencing, and anthropogenic masking reduces false positives and strengthens interpretation.

While limitations remain – including cloud contamination, atmospheric noise, and temporal resolution gaps – the approach offers operational potential. Future research should expand automated anomaly detection, test multi-indicator thresholds, and apply this framework to other active volcanoes in Europe.

All analytical workflows were implemented in open-source environments (Google Earth Engine and SNAP), ensuring full reproducibility. Future research will integrate automated anomaly detection pipelines to strengthen operational use in real-time volcanic monitoring.

Abbreviations

The following abbreviations are used in this manuscript:

NDVI	Normalized Difference Vegetation Index
EVI	Enhanced Vegetation Index
NBR	Normalized Burn Ratio
NDMI	Normalized Difference Moisture Index
InSAR	Interferometric Synthetic Aperture Radar
DInSAR	Differential Interferometric Synthetic Aperture Radar
SBAS	Small Baseline Subset
SNAP	Sentinel Application Platform
GEE	Google Earth Engine
SCL	Scene Classification Layer
TIR	Thermal Infrared
SO_2	Sulfur Dioxide
NO_2	Nitrogen Dioxide
CO	Carbon Monoxide
ROI	Region of Interest
LOS	Line of Sight
SRTM	Shuttle Radar Topography Mission
GNSS	Global Navigation Satellite System
ERA5	ECMWF Reanalysis v5 (meteorological data)
GACOS	Generic Atmospheric Correction Online Service
QA	Quality Assurance (TROPOMI data flag)
DU	Dobson Unit (SO_2 thresholding)
VONA	Volcano Observatory Notice for Aviation
EO Browser	Earth Observation Browser (Copernicus)
S5P/TROPOMI	Sentinel-5 Precursor / TROPOspheric Monitoring Instrument

References

Albino, F., Biggs, J., Yu, C., & Li, Z. (2020). Automated Methods for Detecting Volcanic Deformation Using Sentinel-1 InSAR Time Series Illustrated by the 2017-2018 Unrest at Agung, Indonesia. *Journal of Geophysical Research: Solid Earth*, *125*(2). https://doi.org/10.1029/2019JB017908

Biggs, J., Anantrasirichai, N., Anderson, K., Cayol, V., Dualeh, E., Dumont, Q., Ebmeier, S., Froger, J. L., Gaddes, M., Galetto, F., Gonzalez, P., Hamling, I., Hooper, A., Lazecky, M., & Pritchard, M. (2025). *Rapid Advances in Volcano Monitoring Driven by the First Decade of Sentinel-1 Observations*.

Braun, A., & Veci, L. (2021). *Sentinel-1 Toolbox TOPS Interferometry Tutorial*.

Bruno, V., Aloisi, M., Gambino, S., Mattia, M., Ferlito, C., & Rossi, M. (2022). The Most Intense Deflation of the Last Two Decades at Mt. Etna: The 2019-2021 Evolution of Ground Deformation and Modeled Pressure Sources. *Geophysical Research Letters*, *49*(6). https://doi.org/10.1029/2021GL095195

Cofano, A., Cigna, F., Amato, L. S., Sicilini de Cumis, M., & Tapete, D. (2021). Exploiting Sentinel-5P TROPOMI and Ground Sensor Data for the Detection of Volcanic SO_2 Plumes and Activity in 2018-2021 at Stromboli, Italy. *Sensors*, *21*(21), 6991. https://doi.org/10.3390/s21216991

Corradino, C., Jouve, P., La Spina, A., & Del Negro, C. (2024). Monitoring Earth's atmosphere with Sentinel-5 TROPOMI and Artificial Intelligence: Quantifying volcanic SO_2 emissions. *Remote Sensing of Environment*, *315*. https://doi.org/10.1016/j.rse.2024.114463

Dozzo, M., Aiuppa, A., Bilotta, G., Cappello, A., & Ganci, G. (2025). A New Algorithm for the Global-Scale Quantification of Volcanic SO_2 Exploiting the Sentinel-5P TROPOMI and Google Earth Engine. *Remote Sens.*, *17*(3). https://doi.org/10.3390/rs17030534

Ferretti, A., Monti-Guarnieri, A., Prati, C., Rocca, F., & Massonet, D. (2007). *InSAR Principles: Guidelines for SAR Interferometry Processing and Interpretation*. ESA TM-19. ISBN: 92-9092-233-8.

Furtney, M. A., Pritchard, M. E., Biggs, J., Carn, S. A., Ebmeier, S. K., Jay, J. A., McCormick Kilbridge, B. T., & Reath, K. A. (2018). Synthesizing multi-sensor, multi-satellite, multi-decadal datasets for global volcano monitoring. *Journal of Volcanology and Geothermal Research*, *365*. https://doi.org/10.1016/j.jvolgeores.2018.10.002

Geudtner, D., Torres, R., Snoeij, P., Davidson, M., & Rommen, B. (2014). *Sentinel-1 System capabilities and applications*. IEEE Geoscience and Remote Sensing Symposium, Quebec City, QC, Canada, pp. 1457-1460. https://doi.org/10.1109/IGARSS.2014.6946711

Iacono, F., Bisson, M., Spinetti, C., & Kwasnitschka, T. (2025). Wildfires Induced by Volcanic Activity at Stromboli Island during the 2019 Summer through Satellite and Drone Data. *Remote Sens Earth Syst Sci*, *8*, 733-752. https://doi.org/10.1007/s41976-025-00215-6

Kancheva, R., & Borisova, D. (2006). *Vegetation stress indicators derived from multispectral and multitemporal data*. AIAA 2006-B1.P.1.02. 57th International Astronautical Congress. https://doi.org/10.2514/6.IAC-06-B1.P.1.02

Lange, K., Richter, A., Schönhardt, A., Meier, A. C., Bösch, T., Seyler, A., Krause, K., Behrens, L. K., Wittrock, F., Merlaud, A., Tack, F., Fayt, C., Friedrich, M. M., Dimitropoulou, E., Van Roozendael, M., Kumar, V., Donner, S., Ziegler, S., Lauster, B., Razi, M., Borger, C., Uhlmannsiek, K., Wagner, T., Ruhtz, T., Eskes, H., Bohn, B., Diaz, D. S., Abuhassan, N., Schuettemeyer, D., & Burrows, J. P. (2023). Validation of Sentinel-5P TROPOMI tropospheric NO_2 products by comparison with NO_2 measurements from airborne imaging DOAS, ground-based stationary DOAS, and mobile car DOAS measurements during the S5P-VAL-DE-Ruhr campaign. *Atmospheric Measurement Techniques*, *16*(5). https://doi.org/10.5194/amt-16-1357-2023

Paez, P. A., Cogliati, M. G., Caselli, A. T., & Monasterio, A. M. (2021). An analysis of volcanic SO_2 and ash emissions from Copahue volcano. *Journal of South American Earth Sciences*, *110*. https://doi.org/10.1016/j.jsames.2021.103365

Plank, S., Shevchenko, A. V., d'Angelo, P., Gstaiger, V., González, P. J., Cesca, S., Martinis, S., & Walter, T. R. (2023). Combining thermal, tri-stereo optical and bi-static InSAR satellite imagery for lava volume estimates: the 2021 Cumbre Vieja eruption, La Palma. *Scientific Reports*, *13*, 2057. https://doi.org/10.1038/s41598-023-29061-6

Pritchard, M. E., Poland, M., Reath, K., Andrews, B., Bagnardi, M., Biggs, J., Carn, S., Coppola, D., Ebmeier, S. K., Furtney, M. A., Girona, T., Griswold, J., Lopez, T., Lundgren, P., Ogburn, S., Pavolonis, M., Rumpf, E., Vaughan, C., Wauthier, C., Wessels, R., Wright, R., Anderson, K. R., Bato, M. G., & Roman, A. (2022). *Optimizing Satellite Resources for the Global Assessment and Mitigation of Volcanic Hazards—Suggestions from the USGS Powell Center Volcano Remote Sensing Working Group*. Scientific Investigations Report 2022-5116. https://doi.org/10.3133/sir20225116

Strashok, O., Ziemiańska, M., & Strashok, V. (2020). Evaluation and Correlation of Sentinel-2 NDVI and NDMI in Kyiv (2017-2021). *Journal of Ecological Engineering*, *23*(9), 212-218. http://dx.doi.org/10.12911/22998993/151884

Theys, N., Brenot, H., De Smedt, I., Lerot, C., Hedelt, P., Loyola, D., Vlietnick, J., Yu, H., Smets, B., Kervyn, F., Barrière, J., Oth, A., d'Oreye, N., & Van Roozendael, M. (2019). Global Monitoring of Volcanic SO_2 Degassing Using Sentinel-5P Precursor Tropomi. *Scientific Reports*, *9*, 2643. https://doi.org/10.1038/s41598-019-39279-y

Tian, Y., Hong, X., Shan, C., Sun, Y., Wang, W., Zhou, M., Wang, P., Lin, & P., Liu, C. (2022). Investigating the Performance of Carbon Monoxide and Methane Observations from Sentinel-5 Precursor in China. *Remote Sens.*, *14*(23), 6045. https://doi.org/10.3390/rs14236045

Xie, D., Zhang, X., Han, Q., He, Q., Meng, X., Li, F., & Zhou, K. (2019). Uncertainty Analysis on Process Organized Emission Inventory in Petrochemical Enterprises of Hainan Province. *IOP Conf. Ser.: Earth Environ. Sci.*, *295*(5), 052052. https://doi.org/10.1088/1755-1315/295/5/052052